

**Fermi surface evolution through a heavy fermion  
superconductor-to-antiferromagnet transition: de Haas-van  
Alphen effect in Cd-substituted CeCoIn<sub>5</sub>**

C. Capan,<sup>1</sup> Y.-J. Jo,<sup>2</sup> L. Balicas,<sup>2</sup> R. G. Goodrich,<sup>3,\*</sup> J. F.  
DiTusa,<sup>3</sup> I. Vekhter,<sup>3</sup> T. P. Murphy,<sup>2</sup> A. D. Bianchi,<sup>1,†</sup> L.D.  
Pham,<sup>1,‡</sup> J. Y. Cho,<sup>4</sup> J. Y. Chan,<sup>4</sup> D. P. Young,<sup>3</sup> and Z. Fisk<sup>1</sup>

<sup>1</sup>*Department of Physics and Astronomy,*

*University of California Irvine, Irvine, CA 92697-4575*

<sup>2</sup>*National High Magnetic Field Laboratory,*

*Florida State University, Tallahassee, Florida 32310*

<sup>3</sup>*Department of Physics and Astronomy,*

*Louisiana State University, Baton Rouge, Louisiana 70803*

<sup>4</sup>*Department of Chemistry, Louisiana State University, Baton Rouge, Louisiana 70803*

(Dated: December 6, 2018)

**Abstract**

We report the results of de-Haas-van-Alphen (dHvA) measurements in Cd doped CeCoIn<sub>5</sub> and LaCoIn<sub>5</sub>. Cd doping is known to induce an antiferromagnetic order in the heavy fermion superconductor CeCoIn<sub>5</sub>, whose effect can be reversed with applied pressure. We find a slight but systematic change of the dHvA frequencies with Cd doping in both compounds, reflecting the chemical potential shift due to the addition of holes. The frequencies and effective masses are close to those found in the nominally pure compounds with similar changes apparent in the Ce and La compounds with Cd substitution. We observe no abrupt changes to the Fermi surface in the high field paramagnetic state for  $x \sim x_c$  corresponding to the onset of antiferromagnetic ordering at  $H = 0$  in CeCo(In<sub>1-x</sub>Cd<sub>x</sub>)<sub>5</sub>. Our results rule out  $f$ -electron localization as the mechanism for the tuning of the ground state in CeCoIn<sub>5</sub> with Cd doping.

## I. INTRODUCTION

A common thread in unconventional superconductivity is that it emerges close to a quantum critical point (QCP). A QCP is the point in a phase diagram where long-range order is suppressed to zero temperature,  $T = 0$ , by an external parameter other than  $T$  so that quantum, rather than thermal fluctuations drive the transition<sup>1</sup>. One way to rationalize the QCP in heavy fermion metals is the phase diagram proposed by Doniach<sup>2</sup> in which the ground state evolves from a local moment antiferromagnet to a heavy fermion paramagnet as a function of the tuning parameter  $Jg(\varepsilon_F)$ , where  $J$  is the exchange coupling strength and  $g(\varepsilon_F)$  the density of states at the Fermi level. The QCP then corresponds to the point where the Kondo energy scale  $\sim \exp(-\frac{1}{Jg(\varepsilon_F)})$  equals the RKKY scale  $\sim (Jg(\varepsilon_F))^2$ . The quantum-critical spin-fluctuations associated with the suppression of antiferromagnetic order are likely involved in the pairing mechanism for unconventional superconductivity<sup>3,4</sup>. This picture has been considered as an explanation for a broad range of superconductors, including high- $T_c$  cuprates<sup>5</sup>, heavy fermion metals<sup>6-9</sup>, cobaltates<sup>10</sup>, as well as the recently discovered iron-pnictides<sup>11</sup>. However, there are also important exceptions where unconventional superconductivity is observed and no competing magnetic order is found, such as in the cases of  $\text{UBe}_{13}$ <sup>7</sup> and  $\text{Sr}_2\text{RuO}_4$ <sup>12</sup>. There is also the possibility of valence, rather than spin, fluctuation mediated superconductivity as suggested for  $\text{CeCu}_2\text{Si}_2$  under pressure<sup>6</sup>.

Many studies have used doping as a tuning parameter between superconducting and antiferromagnetic ground states in a broad range of strongly correlated electron systems hosting a QCP<sup>10,11,13,14</sup>. The heavy fermion metals in particular are very susceptible to chemical substitution. In these compounds the Kondo coupling between a lattice of local moments and the conduction band creates quasi-particle excitations with large effective masses, and the dopants disrupt the coherent Kondo coupling. Such studies have been essential in assessing the percolative nature in which the coherence in the Kondo lattice emerges -see for example the La-dilution study of  $\text{CeCoIn}_5$ <sup>15</sup>- as well as its sensitivity to disorder<sup>16</sup>. But doping can also tune the ground state by changing the carrier concentration as is remarkably illustrated in the high- $T_c$  cuprates<sup>5</sup>. One important aspect of doping the  $\text{CuO}_2$  layers in the high- $T_c$  cuprates is the apparent electron-hole symmetry: the phase

diagrams are qualitatively similar whether the carriers introduced are electron-like or hole-like. One can then focus on a universal phase diagram as a function of the carrier concentration, without having to investigate the local effects associated with each particular dopant. This symmetry is not found in  $\text{CeCoIn}_5$  and so it is not possible to define a universal phase diagram with doping as we demonstrate below.

$\text{CeCoIn}_5$  is a heavy fermion superconductor<sup>8</sup> where Cooper pairs are formed out of a non-Fermi Liquid metallic state. The divergence observed in the electronic specific heat, as well as the non-quadratic  $T$ -dependence of the resistivity found even at very low temperatures, suggest the presence of a QCP when superconductivity is suppressed by a magnetic field<sup>17,18</sup>. The nature of the QCP has been the subject of much speculation, but it seems likely to be an antiferromagnetic QCP. Hall effect measurements under pressure have shown that the QCP is located not exactly at the upper critical field  $H_{c2}$  but at a slightly lower field<sup>19</sup>. Inelastic neutron scattering<sup>20</sup> and NMR measurements<sup>21</sup>, on the other hand, have revealed the presence of antiferromagnetic fluctuations within the superconducting state. More recently, a field induced antiferromagnetic order coupled to superconductivity has been discovered close to  $H_{c2}$  via neutron scattering<sup>22</sup> and  $\mu\text{SR}$  measurements<sup>23</sup> in pure  $\text{CeCoIn}_5$ .

The ability to grow sizable, high quality, single crystals enables detailed investigation of the effect of chemical doping in this and other 115 compounds. While Sn-doping was found to suppress  $T_c$  without revealing any incipient magnetism<sup>24</sup>, Cd doping induces an antiferromagnetic ground state in  $\text{CeCoIn}_5$ . The same behavior is also observed in the two other stoichiometric  $\text{CeMIn}_5$  ( $M = \text{Rh}, \text{Ir}$ )<sup>25</sup> as well as the bilayer  $\text{Ce}_2\text{MIn}_8$  ( $M = \text{Co}, \text{Rh}, \text{Ir}$ )<sup>26</sup> with Cd doping. Because Sn and Cd are neighbors to In in the periodic table, Sn and Cd substitutions for In result in electron and hole doping, respectively. The effect of Cd is quite unusual in the sense that it takes a very small density of Cd to induce the paramagnetic to antiferromagnetic (AFM) ground state transformation which can be reversed with the application of pressure<sup>25</sup>. How Cd induces long range AFM order with a large ordered magnetic moment<sup>27</sup> ( $0.7\mu_B$  per Ce) in  $\text{CeCoIn}_5$  remains an open question.

One possible mechanism is the formation of antiferromagnetic droplets at the Cd sites, as was inferred from NMR measurements<sup>27</sup>. Long range AFM order occurs once the density of such droplets reaches the percolation threshold. However, the density of Cd necessary to induce ordering is well below the percolation threshold. Thus the ordering at such a small

Cd concentration requires very long correlation length and correspondingly large size of the ordered droplet around each dopant. Thus the ordering at such a small Cd concentration requires interactions with a longer range. Since the ordered moments are likely local moments on the Ce sites, one way to account for the reversibility of Cd doping with pressure is to speculate that the change in carrier density and disorder caused by Cd substitution localizes the  $f$ -electrons of nearby Ce atoms. Application of pressure to metals with localized  $f$ -orbitals tends to increase the hybridization with the conduction band and delocalize  $f$ -electrons.

Alternatively, the AFM state is due to a Fermi Surface (FS) instability, which is the well-known explanation in the case of elemental Cr. Recent neutron scattering results in Cd doped  $\text{CeCoIn}_5$ <sup>28</sup> have demonstrated that the AFM ordering has a wavevector,  $Q$  of  $(1/2, 1/2, 1/2)$  suggesting that if the AFM is nesting-driven, the nesting wavevector is commensurate with the lattice. This is a plausible, but unusual, situation that occurs, for example, in Mn doped Cr<sup>29</sup>. It is possible that in the situation intermediate between local and itinerant the magnetic ordering is driven by the local, unscreened component of the spin, and the improved near-nesting with Cd doping lowers the energy cost of opening the gap for itinerant electrons at the magnetic Brillouin Zone boundary, enabling the long-range order to appear.

Perhaps the most surprising feature of this ordered state is that the ordering wavevector<sup>28</sup> coincides with the wavevector at which an inelastic neutron scattering resonance<sup>20</sup> is observed in the superconducting state of pure  $\text{CeCoIn}_5$ . The origin of this resonance has been attributed to AFM magnons<sup>30</sup> and we suspect the coincidence is not accidental. A similar AFM state can be induced with Rh substitution for Co in  $\text{CeCoIn}_5$  for Rh concentrations greater than  $\sim 25\%$ <sup>31</sup>. Here, the AFM wavevector is identical to that found for Cd doped  $\text{CeCoIn}_5$ , which coexists with superconductivity for Rh concentrations of less than  $\sim 60\%$ . For larger Rh concentrations the AFM wavevector becomes  $(1/2, 1/2, \sim 0.3)$  and superconductivity is suppressed. The change in wavevector and the loss of superconductivity at Rh concentrations above 60% suggest that the AFM state in Rh (for  $x_{Rh} < 0.6$ ) and Cd doped  $\text{CeCoIn}_5$  has a different character from the local moment antiferromagnetism found in  $\text{CeRhIn}_5$ . In order to understand more fully the superconducting state in  $\text{CeCoIn}_5$  and the relevance of the nearby AFM QCP, the character of the AFM state will require further investigations.

In this paper, we report on one such investigation by specifically exploring the evolution

of the FS of both CeCoIn<sub>5</sub> and LaCoIn<sub>5</sub> as a function of Cd doping via de Haas van Alphen (dHvA) oscillations. We observe that the changes to the FS with Cd substitution are consistent with the addition of holes and that the FS varies with Cd substitution at a similar rate in both compounds. Our results thus rule out *f*-electron localization as a possible route towards AFM order. If this were the case it would lead to a significantly different evolution of the Fermi surfaces of CeCo(In<sub>1-x</sub>Cd<sub>x</sub>)<sub>5</sub> and the non-magnetic La-analog. This paper is organized as follows: We first present the experimental details in section II followed by an introduction to the phase diagram in section III. Section IV focuses on the evolution of the Fermi Surface in Cd doped CeCoIn<sub>5</sub> in comparison to Cd doped LaCoIn<sub>5</sub> while section V presents the effect of Cd on the cyclotron effective mass and mean free path. We summarize our findings in section VI and discuss the possible mechanism(s) for AFM order in Cd doped CeCoIn<sub>5</sub> that is (are) consistent with our data.

## II. EXPERIMENTAL DETAILS

The single crystals of CeCo(In<sub>1-x</sub>Cd<sub>x</sub>)<sub>5</sub> and LaCo(In<sub>1-x</sub>Cd<sub>x</sub>)<sub>5</sub> used in our experiments are grown from In flux in a ratio of Ln:Co:In:Cd (1 : 1 : 20(1 - *x*) : 20*x*) from high purity starting materials, as described elsewhere<sup>8</sup>. The lattice parameters were determined by using both powder and single crystal X-ray diffraction and are shown in figure 1a. Si was used as a standard in the Rietveld refinement of the powder X-ray diffraction patterns. We have determined the Cd concentration via Energy Dispersive X-ray analysis (EDS) resulting in values comparable to those published by other groups<sup>32</sup>. These measurements indicate that only a fraction of the Cd ( $\sim 30\%$ ) effectively substitutes for In, as we found  $x = 1.6, 1.9$  and  $2.3\%$  for nominal concentrations of  $x = 2.5, 5$  and  $7.5\%$  in CeCo(In<sub>1-x</sub>Cd<sub>x</sub>)<sub>5</sub>. Similarly, we obtained  $x = 1.3, 1.6, 2.2$  and  $2.3\%$  for nominal concentrations of  $x = 2.5, 5, 7.5$  and  $10\%$  in LaCo(In<sub>1-x</sub>Cd<sub>x</sub>)<sub>5</sub>. For ease of comparison with previous work we quote the nominal concentrations throughout the paper.

The susceptibility of single crystals of CeCo(In<sub>1-x</sub>Cd<sub>x</sub>)<sub>5</sub> was measured at  $H = 0.1$  T applied perpendicular to [001] for temperatures ranging from 1.8 to 400 K using a commercial vibrating sample Superconducting Quantum Interference Device (SQUID) magnetometer. The Curie-Weiss parameters were obtained from fits to susceptibility in the  $T$ -range of 100 – 400 K and are shown in figure 1b. For the concentrations for which more than one

sample was measured, the average values are shown and the error bars correspond to the standard deviation. The resistivity was measured from 1.8 to 300 K at  $H = 0$  with a current of 1 mA applied along [100] in single crystals of  $\text{CeCo}(\text{In}_{1-x}\text{Cd}_x)_5$  for  $x = 5, 10$  and 15%. The crystals were In free and the Pt wires were attached using silver epoxy.

The evolution of the FS of the same crystals used for the single crystal X-ray diffraction measurements was investigated via the Fast Fourier Transform (FFT) analysis of the dHvA oscillations measured using a torque magnetometer<sup>33</sup>. Single crystals were mounted on a Cu-Be cantilever, inside either a  $^3\text{He}$  cryostat or a dilution refrigerator equipped with a rotator. The torque signal was measured at the National High Magnetic Field Laboratory, using a capacitance bridge in magnetic fields of up to 35 T, and for temperatures down to 0.3 K and 0.05 K for the  $\text{LaCo}(\text{In}_{1-x}\text{Cd}_x)_5$  and the  $\text{CeCo}(\text{In}_{1-x}\text{Cd}_x)_5$  crystals, respectively. For the FFT analysis it is assumed that  $H \approx B$  without demagnetizing factor correction, since we estimate the magnetization of  $\text{CeCo}(\text{In}_{1-x}\text{Cd}_x)_5$  to be  $\sim 0.4\%$  of the applied field. Indeed, the in-plane susceptibility (measured down to 1.8 K) is extrapolated with a power law fit to  $\chi_{\perp} = 0.0143$  emu/mol at  $T = 50$  mK in 5%Cd doped  $\text{CeCoIn}_5$ , which corresponds to  $\chi_{\parallel} = 0.0286$  emu/mol for  $H \parallel [001]$  (with a magnetic anisotropy of 2) and to a volume magnetization of  $4\pi M = 1260$  G at 35 T.

Fig. 1a shows the change in lattice parameters as a function of the nominal Cd concentration in  $\text{LaCo}(\text{In}_{1-x}\text{Cd}_x)_5$  and  $\text{CeCo}(\text{In}_{1-x}\text{Cd}_x)_5$  where we observe that the main effect of Cd substitution is to produce a volume contraction in both compounds. This is as expected since Cd atoms are smaller than In atoms. The volume contraction rate is similar in both the Ce and the La compounds and is in quantitative agreement with the contraction inferred from a local structure, extended X-ray absorption fine structure (EXAFS), investigations<sup>34</sup> for the same nominal concentrations. EXAFS results also indicate that Cd, as well as Sn, preferentially substituted for In on the in-plane, In(1), site<sup>34</sup>. The close agreement between the powder and the single crystal X-ray lattice parameters (see fig. 1a) suggest that the variation of the Cd concentration within a batch is small: we estimate a difference of  $\Delta x \leq 2\%$  between single crystal and average (powder) nominal concentrations.

The similar suppression of the unit cell volume in both the Ce- and the La-compounds apparent in Fig. 1a indicates that Cd doping has no significant effect on the valence of Ce at room  $T$ . If the addition of Cd were to change the valence of Ce, the size of the Ce ions, and consequently the lattice parameters of  $\text{CeCo}(\text{In}_{1-x}\text{Cd}_x)_5$ , would have a rather distinct

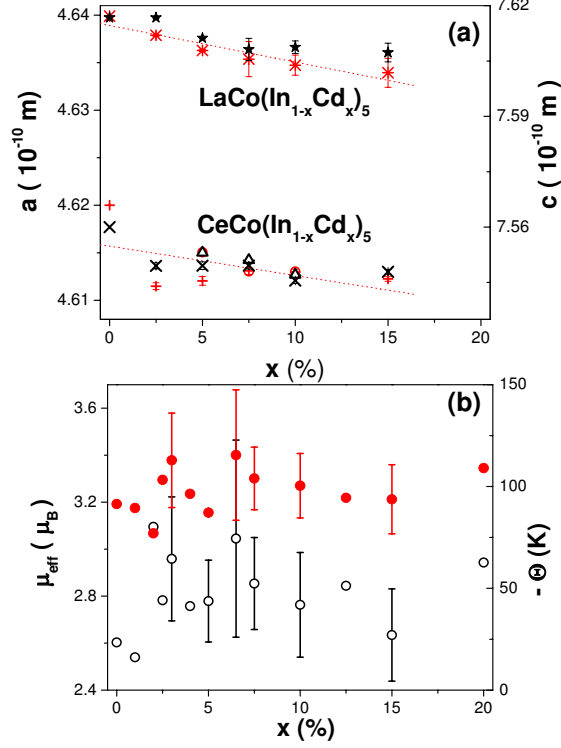


FIG. 1: (Color online) (a) Lattice parameters  $a$  and  $c$  along [100] and [001] respectively vs nominal Cd concentration  $x$  in  $\text{LaCo}(\text{In}_{1-x}\text{Cd}_x)_5$  ( $*$  :  $a$ ,  $\star$  :  $c$ ) and  $\text{CeCo}(\text{In}_{1-x}\text{Cd}_x)_5$  ( $+$  :  $a$ ,  $\times$  :  $c$ ) obtained from powder X-ray diffraction. Single crystal X-ray diffraction results are also shown for  $x = 5\%$ ,  $7.5\%$  and  $10\%$  in  $\text{CeCo}(\text{In}_{1-x}\text{Cd}_x)_5$  ( $\circ$  :  $a$ ,  $\triangle$  :  $c$ ). The error bars are smaller than the symbol size where they are not shown. The dotted lines are linear fits to  $a$  vs  $x$ . (b) Curie-Weiss moment  $\mu_{eff}$  ( $\circ$ ) and Curie-Weiss Temperature  $\Theta$  ( $\bullet$ ) vs nominal Cd concentration  $x$  in  $\text{CeCo}(\text{In}_{1-x}\text{Cd}_x)_5$ . The Curie-Weiss parameters were obtained from fits to the susceptibility in the  $T$ -range of  $100 - 400$  K, measured with  $H = 0.1$  T applied perpendicular to [001]. For concentrations in which more than one sample was measured average values are shown with error bars corresponding to the standard deviations.

doping dependence in comparison to their La-analogs. This is also supported by the lack of a systematic variation of either the effective Curie moment or the Weiss temperature with Cd substitution (Fig. 1b) as determined from the magnetic susceptibility. However, these data do not preclude a possible valence fluctuation scenario at low  $T$ .

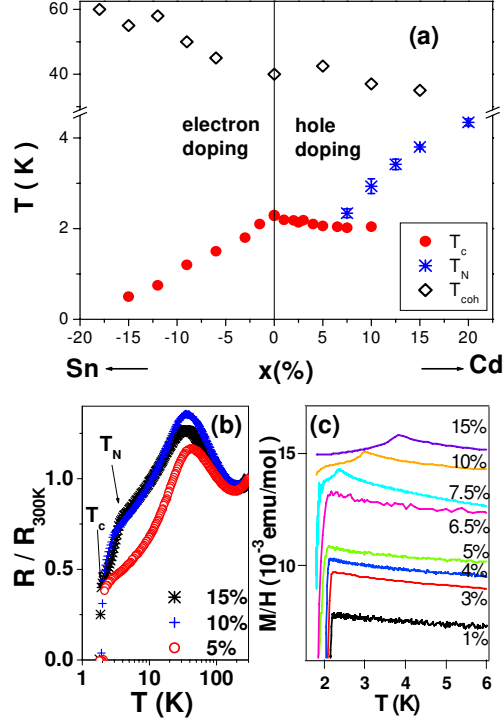


FIG. 2: (Color online) Phase diagram. (a) Temperature,  $T$  vs. doping,  $x$  phase diagram of  $\text{CeCo}(\text{In}_{1-x}\text{M}_x)_5$ ,  $\text{M}=\text{Sn}, \text{Cd}$ . The Sn and Cd concentrations are nominal. The superconducting ( $T_c, \bullet$ ) and the antiferromagnetic ( $T_N, *$ ) transition temperatures for Cd doped samples are obtained from magnetic susceptibility. The Kondo coherence temperature ( $T_{coh}, \diamond$ ) corresponds to the resistivity maximum.  $T_{coh}$  and  $T_c$  for Sn doped samples are from ref. 35. (b) Normalized resistance,  $R/R_{300K}$  vs.  $T$  from 1.8 to 300 K on a semi-log plot at  $H = 0$  for single crystals of  $\text{CeCo}(\text{In}_{1-x}\text{Cd}_x)_5$  with  $x = 5, 10$  and 15%. (c) Magnetic susceptibility,  $M/H$  vs.  $T$  at  $H = 0.1$  T in  $\text{CeCo}(\text{In}_{1-x}\text{Cd}_x)_5$  in the range 1.8 – 6 K showing the superconducting and antiferromagnetic transitions. Nominal Cd concentrations are indicated in the figure. The  $x = 5, 10\%$  and 15% data have been shifted by  $2, 5$  and  $6 \times 10^{-3}$  emu/mol vertically for clarity.

### III. THE PHASE DIAGRAM

The doping dependent phase diagram of  $\text{CeCo}(\text{In}_{1-x}\text{Cd}_x)_5$  is shown in Fig. 2a together with the resistivity and the magnetic susceptibility in Fig. 2b and 2c. The superconducting critical temperature  $T_c$  and the Neel temperature  $T_N$  are determined from the sharp drop and the peak in the magnetic susceptibility, respectively (see Fig. 2c). These are consistent with the transitions seen in the resistivity at  $H = 0$  (see Fig. 2b). Fig. 2a includes the



Sn-doping phase diagram<sup>35</sup> for comparison. Superconductivity is suppressed with both Sn and Cd doping as a result of pair-breaking via impurity scattering, although this suppression appears to be stronger with Sn than for Cd dopants. Antiferromagnetic order sets-in for  $x \geq 7.5\%$  for Cd doping only, emphasizing the electron-hole asymmetry in the doping phase-diagram of CeCoIn<sub>5</sub>.

The overall phase diagram as a function of Cd doping obtained by us is consistent with a previous report<sup>25</sup>, and in particular with a finite range of coexistence for both the superconducting and AFM phases. While the samples with  $x = 7.5\%$  systematically show both superconducting and AFM transitions, traces of superconductivity are also observed for  $x = 10\%$ , as seen in Fig. 2c, although this is highly sample dependent. The superconducting transition is also observed in the  $H = 0$  resistivity (see Fig. 2b) for our  $x = 10$  and  $15\%$  crystals. This suggests that the doping may be somewhat inhomogeneous within a given single crystal. Nevertheless, a microscopic coexistence of both orders has been claimed based on neutron scattering and NMR measurements<sup>27,28</sup>. The evolution of transition temperatures  $T_c$  and  $T_N$  with Cd doping remains quite systematic (see Fig. 2a) with only a small variation observed within a given batch. Superconductivity coexisting with a commensurate AFM order appears to be a generic feature of doped CeCoIn<sub>5</sub> since it was also observed with Rh substitution<sup>31,36</sup> for  $x_{Rh} < 0.6$ .

The Kondo coherence temperature  $T_{\text{coh}}$  in CeCo(In<sub>1-x</sub>Cd<sub>x</sub>)<sub>5</sub>, as determined from the maximum in the resistivity as a function of temperature (see Fig. 2b), is displayed in Fig. 2a. The Cd doping tends to suppress  $T_{\text{coh}}$ , a trend which is the opposite to the effect of Sn doping<sup>35</sup> which is included in Fig. 2a for comparison. Since  $T_{\text{coh}}$  increases with pressure<sup>37</sup> one way of rationalizing the evolution of the  $T_{\text{coh}}$  with Sn and Cd doping is in terms of the lattice volume change. However, the enhancement of  $T_{\text{coh}}$  with Sn doping is not simply a chemical pressure effect since Sn has no detectable effect on the lattice volume<sup>35</sup>. Nor is the suppression of  $T_{\text{coh}}$  specific to Cd: a recent investigation on rare-earth substitution has shown that  $T_{\text{coh}}$  is systematically suppressed as the Ce lattice is diluted, regardless of the magnetic or electronic nature of the rare-earth dopants<sup>16</sup>. This fact, taken alone, may seem to suggest that the small suppression of  $T_{\text{coh}}$  with Cd doping is effectively a dilution effect as Cd localizes the f-electrons on a small number of neighboring Ce ions. As we see below, this is not supported by our measurements. Moreover, there is an important difference in that both Yb<sup>38</sup> and Cd<sup>25</sup> act as hole dopants but only Cd stabilizes the AFM state in CeCoIn<sub>5</sub>.

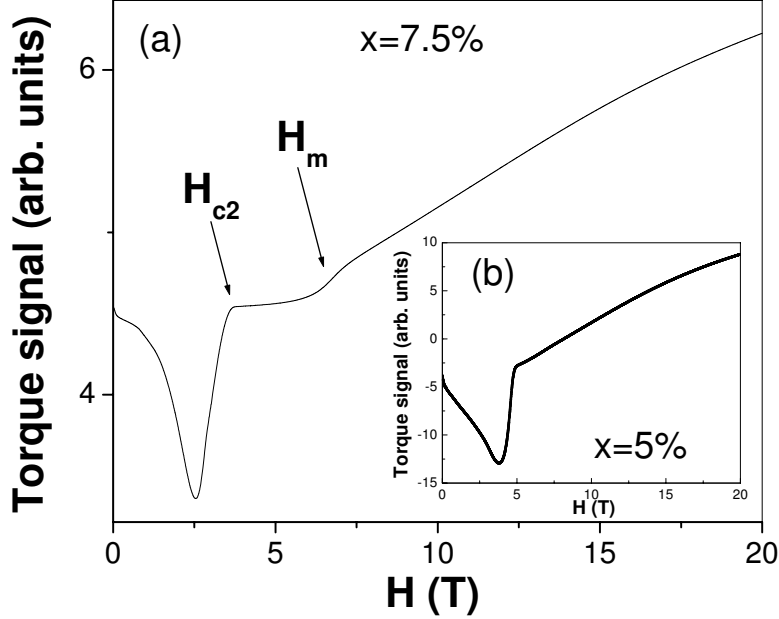


FIG. 3: Torque signal. Torque signal vs magnetic field in  $\text{CeCo}(\text{In}_{1-x}\text{Cd}_x)_5$  at  $T = 0.05$  K for  $x = 7.5\%$  (a) and  $5\%$  (b). The torque signal is proportional to magnetization<sup>33</sup>. The magnetic field is oriented at  $8^\circ$  from  $[001]$ .  $H_{c2}$  and  $H_m$  correspond to the superconducting upper critical field and the metamagnetic transition respectively.

The opposing effects of Sn and Cd instead suggest that the changes to  $T_{\text{coh}}$  are a consequence of the shift in the chemical potential corresponding to electron or hole doping.

Tuning the ground state with Cd does not appear to conform to the Doniach phase diagram of competing RKKY and Kondo scales<sup>2</sup> since no systematic change is observed in either the Curie-Weiss temperature (see Fig. 1b), a measure of the RKKY interaction strength, nor the single-ion Kondo scale, determined from the magnetic entropy of a series of 5% Ce doped  $\text{LaCo}(\text{In},\text{Cd})_5$  crystals (not shown), with Cd substitution. NMR measurements<sup>27</sup> also indicate an absence of change to the low energy spin fluctuation spectrum with Cd substitution in  $\text{CeCoIn}_5$  in the paramagnetic state. Thus, the natural question is whether the Cd-induced antiferromagnetism is, instead, due to a Fermi surface instability, a possibility we investigate via the dHvA measurements presented below.

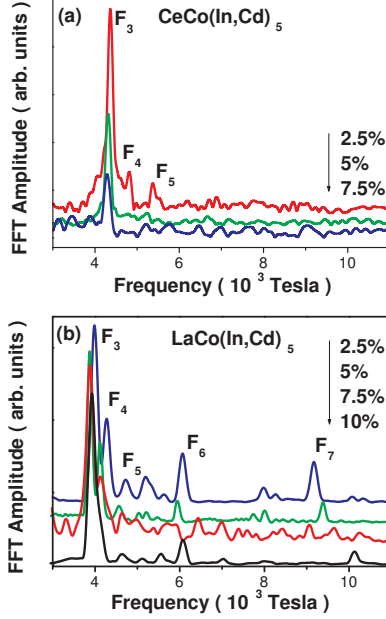


FIG. 4: (Color online) de Haas-van Alphen Spectrum. Fast Fourier Transform (FFT) vs Frequency in: (a)  $\text{CeCo}(\text{In}_{1-x}\text{Cd}_x)_5$  and (b)  $\text{LaCo}(\text{In}_{1-x}\text{Cd}_x)_5$ . The nominal concentrations of  $x = 2.5\%$ ,  $5\%$ ,  $7.5\%$  and  $10\%$  are indicated. The spectra shown for each concentration is taken for magnetic field oriented at an angle  $\Theta \leq 15^\circ$  from  $[001]$ , at  $T = 0.05$  K and  $T = 0.3$  K for  $\text{CeCo}(\text{In}_{1-x}\text{Cd}_x)_5$  and  $\text{LaCo}(\text{In}_{1-x}\text{Cd}_x)_5$  respectively. The peaks  $F_3, F_4, F_5$  ( $F_6, F_7$ ) correspond to the electron (hole) sheets of the Fermi Surface.

#### IV. THE FERMI SURFACE

To investigate the changes to the Fermi surface with Cd substitution that coincide with the variations noted above, we have systematically measured the dHvA oscillations as a function of  $x$ ,  $T$ , and the magnitude and direction of  $H$ . Figure 3 shows the torque signal (in arbitrary units) as a function of magnetic field between 0 and 20 T oriented at  $8^\circ$  from  $[001]$  at 0.05 K in  $\text{CeCo}(\text{In}_{1-x}\text{Cd}_x)_5$  for  $x = 5$  and  $7.5\%$ . At these low fields dHvA oscillations are not yet apparent. While both samples exhibit a pronounced dip in the vortex state, there is a distinct metamagnetic anomaly at  $H_m \simeq 7$  T  $>$   $H_{c2}$  for the  $x = 7.5\%$  sample, corresponding to the transition from the antiferromagnetic to the paramagnetic state. A maximum in the transverse MR of an  $x = 0.1$  sample is observed at around the same field (not shown). Thus, it appears that for fields large enough for dHvA oscillations to be detected the samples are in the high field paramagnetic state, rather than in the zero field AFM phase. This restriction

precludes the observation of a Fermi surface reconstruction in the magnetic Brillouin zone of the AFM state. Despite this limitation we can learn much about the Fermi surface and the mechanism for AFM in  $\text{CeCo}(\text{In}_{1-x}\text{Cd}_x)_5$  from our dHvA measurements.

Figure 4 shows the Fast Fourier Transform (FFT) of the torque signal (after background subtraction) as a function of frequency in  $\text{CeCo}(\text{In}_{1-x}\text{Cd}_x)_5$  and  $\text{LaCo}(\text{In}_{1-x}\text{Cd}_x)_5$  for all Cd concentrations measured. The FFT is calculated on the same field range 25-35 T for all samples and all orientations. No dHvA oscillations are resolved in  $\text{CeCo}(\text{In}_{1-x}\text{Cd}_x)_5$  for  $x \geq 10\%$  for fields up to 45 T and for temperatures down to 0.05 K. The peaks in the FFT spectra shown in Fig. 4 correspond to the branches of the electron and hole sheets of the Fermi surface that have been previously identified<sup>39,40</sup>. The labeling of these branches is identical to Ref. 40. Overall, similar branches are observed in both Ce and La analogs, with systematically larger frequencies in the Ce compounds as compared to their La counterparts. This is also the case for pure  $\text{CeCoIn}_5$  and is due to the itinerant nature of the  $4f$  electrons in the sense that they are hybridized with the conduction bands<sup>41,42</sup>. In contrast, the FS of the antiferromagnetic compound  $\text{CeRhIn}_5$  is known to be very close to its non-magnetic analog  $\text{LaRhIn}_5$ , suggesting localized  $f$ -electrons<sup>41,42</sup>. The incommensurate AFM order with a large moment  $\mu \sim 0.8 \pm 0.1\mu_B$ , in  $\text{CeRhIn}_5$ <sup>43</sup> is therefore a local moment ordering similar to the incommensurate local moment magnetism found in other rare-earths metals<sup>44</sup>.

The angular dependence of several dHvA branches is shown for  $\text{CeCo}(\text{In}_{1-x}\text{Cd}_x)_5$  in figure 5. No significant change is observed with Cd doping. It was previously established that for nominally pure  $\text{CeCoIn}_5$  the angular dependence for most branches is well described by a  $1/\cos\Theta$  dependence indicative of a quasi-two dimensional Fermi surface<sup>39,40</sup> and this continues to be true for the Cd doped samples.

The evolution of the dHvA frequencies with  $x$  for  $H \parallel [001]$  is shown in figure 6 for  $\text{CeCo}(\text{In}_{1-x}\text{Cd}_x)_5$  (panels *a, b*) and  $\text{LaCo}(\text{In}_{1-x}\text{Cd}_x)_5$  (panels *c, d*). The values reported in the figure correspond to the minimum of the frequency vs angle curves obtained via quadratic fits to the data in fig. 5. The  $\text{LaCo}(\text{In}_{1-x}\text{Cd}_x)_5$  frequencies compare well with those previously reported for pure  $\text{LaCoIn}_5$ <sup>45</sup>, also shown in fig. 6. We have included data for nominally pure  $\text{CeCoIn}_5$  (full symbols) and  $\text{CeRhIn}_5$  (open symbols) for the same branches and orientation ( $H \parallel [001]$ ) taken from the literature<sup>39-42</sup> in fig. 6. This comparison of the dHvA frequencies for these two systems demonstrates that the substantial differences, which were independently observed by two groups<sup>41,42</sup>, are real and beyond experimental

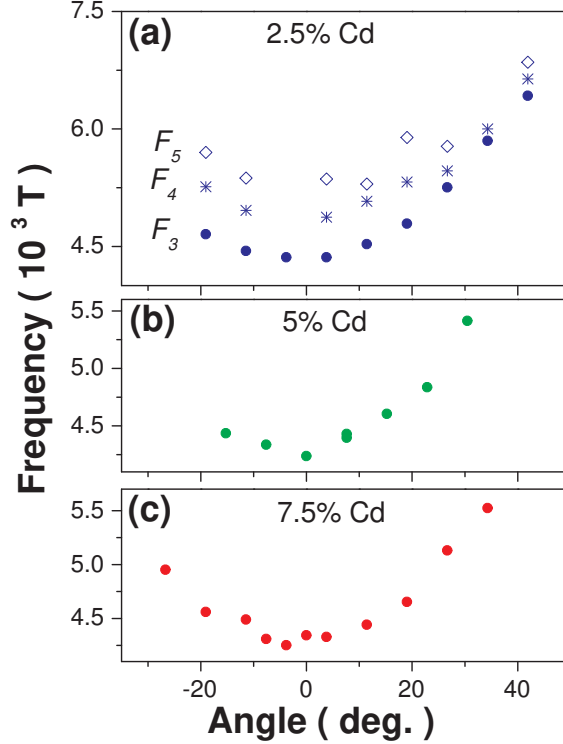


FIG. 5: (Color online) dHvA Frequency vs. Angle in  $\text{CeCo}(\text{In}_{1-x}\text{Cd}_x)_5$ . Angular dependence shown for a)  $x = 2.5\%$ , b)  $x = 5\%$  and c)  $x = 7.5\%$ . Only the  $F_3$  branch is resolved in the  $x = 5\%$  and  $7.5\%$  samples. Zero angle corresponds to  $H \parallel [001]$ .

uncertainty. The conclusion is that in  $\text{CeCoIn}_5$  the dHvA frequencies correspond to a "large" Fermi Surface which includes a contribution from itinerant  $f$ -electrons, whereas in  $\text{CeRhIn}_5$  the dHvA frequencies correspond to a "small" Fermi Surface expected in the case of well localized  $f$ -electrons..

In Fig. 6 we observe that the dHvA frequencies of  $\text{CeCo}(\text{In}_{1-x}\text{Cd}_x)_5$  remain very close to those of the pure  $\text{CeCoIn}_5$  with no abrupt change to  $F_3$  at the critical concentration,  $x_c = 7.5\%$ . In fact, the rate at which the  $F_3$  frequency (electron orbit) is suppressed with Cd is very similar, within the limits of our measurements, in the Ce and the La analogs as emphasized by the linear fits in Fig. 6. These observations tend to rule out any change in the Ce valence at the lowest temperatures, as was inferred at room  $T$  from the lattice parameter evolution. Indeed, if the Ce valence, or simply the hybridization of the  $4f$  electron with the conduction band through Kondo effect, changed with Cd in such a way that the  $4f$  electron was more localized, the effective number of carriers introduced on the Fermi surface by each Cd would *not* be one hole as is expected to be for the case of  $\text{LaCo}(\text{In}_{1-x}\text{Cd}_x)_5$ . One would

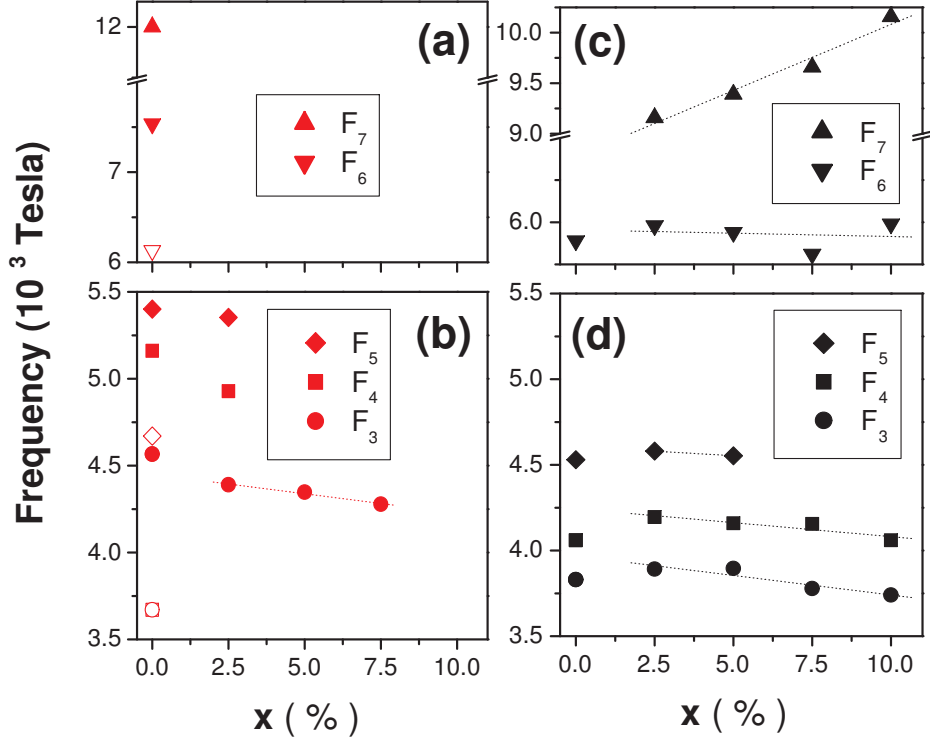


FIG. 6: (Color online) Cd concentration dependence of dHvA spectra. dHvA Frequency vs. nominal Cd concentration in  $\text{CeCo}(\text{In}_{1-x}\text{Cd}_x)_5$  (panels *a, b*) and  $\text{LaCo}(\text{In}_{1-x}\text{Cd}_x)_5$  (panels *c, d*). The upper (lower) panels *a, c* (*b, d*) correspond to the various frequencies of the hole (electron) sheet of the Fermi Surface for  $H \parallel [001]$ , as indicated. The frequencies for pure  $\text{CeCoIn}_5$ ,  $\text{LaCoIn}_5$  and  $\text{CeRhIn}_5$  (open symbols) are from previously published dHvA data<sup>39–42,45</sup>. The dotted lines are linear fits to the data.

then expect the  $F_3$  branch to decrease at a faster rate in  $\text{CeCo}(\text{In}_{1-x}\text{Cd}_x)_5$  when compared to its La-analog. This suggests that the FS of the  $x_c = 7.5\%$  sample is significantly larger than that of the antiferromagnetic counterpart  $\text{CeRhIn}_5$  and rules out the localization of  $f$ -electrons at the onset of antiferromagnetism at  $H = 0$ . The nucleation of a local moment AFM state at  $x_c$  with a large ordered moment,  $\mu = 0.7\mu_B$  per Ce, would require a substantial density of localized Ce  $f$ -electrons. This, in turn, would require a substantial change in the dHvA frequencies, of order the difference between  $\text{CeCoIn}_5$  and  $\text{CeRhIn}_5$ , with Cd doping. The similar evolution of the Fermi Surface in  $\text{CeCo}(\text{In}_{1-x}\text{Cd}_x)_5$  and its La analogs suggests that the effect of Cd is primarily a rigid band shift (or equivalently a shift in the chemical potential) due to the additional hole in *both* systems, without significant change in the Ce valence or the Kondo hybridization of the  $4f$  electron.

This is perhaps the most important finding of our investigation; the  $f$ -electrons in  $\text{CeCo}(\text{In}_{1-x}\text{Cd}_x)_5$  remain itinerant with Cd doping. This is in stark contrast to the naive expectation based upon the similarities in critical temperatures and sizes of magnetic moments,  $\mu$ , that the mechanism for magnetism in  $\text{CeCo}(\text{In}_{1-x}\text{Cd}_x)_5$  at  $x > x_c$  and  $\text{CeRhIn}_5$  are identical. In  $\text{CeRhIn}_5$  the magnetism has been shown to be due to RKKY coupling of the well localized Ce  $f$ -electron magnetic moments, with an incommensurate wavevector<sup>43</sup>. In  $\text{CeCo}(\text{In}_{1-x}\text{Cd}_x)_5$  the antiferromagnetism is commensurate<sup>28</sup> and the large Fermi surface we observe is a further indication that the mechanism driving the magnetism may be quite different from  $\text{CeRhIn}_5$ : the magnetic order involves SDW-like rearrangement of the Fermi surface, rather than a dramatic change in volume as in the  $f$ -electron localization scenario. That the Ce  $f$ -electrons remain well hybridized with the conducting electrons is indicated by the large coherence temperatures seen in Fig. 2 and the insensitivity of the dHvA frequencies to Cd doping. Thus, we reach a conclusion similar to that of a recent investigation of Rh-doped  $\text{CeCoIn}_5$  which indicated no change of the  $F_3$  frequency with Rh doping through the Rh concentration,  $x \sim 25\%$ , for which a commensurate AFM order sets in. The insensitivity of this dHvA frequency to Rh doping also implies a "large" Fermi surface for Rh concentrations where superconductivity coexists with the commensurate AFM order<sup>46</sup>.

The second important finding is that the evolution of dHvA frequencies with Cd doping is opposite for the electron and the hole Fermi Surface sheets in  $\text{LaCo}(\text{In}_{1-x}\text{Cd}_x)_5$  (Fig. 6). In Fig. 6c and d we observe a systematic variation with  $x$  in some of the dHvA frequencies: the frequency of the electron orbits  $F_3, F_4$  decrease, while that of the hole orbit,  $F_7$ , increases with increasing  $x$ . This suggests that the electron Fermi surface ( $F_3, F_4$ ) shrinks for increasing Cd concentration, while the hole Fermi surface ( $F_7$ ) expands. Note that the  $F_6$  orbit, which derives from the same hole FS, is relatively constant suggesting the expansion of the hole sheet is not uniform. Overall, the FS evolution in  $\text{LaCo}(\text{In}_{1-x}\text{Cd}_x)_5$  can be simply understood as a chemical potential shift: Cd effectively is a hole dopant since Cd has one electron less than In.

In the case of  $\text{CeCo}(\text{In}_{1-x}\text{Cd}_x)_5$  we do not observe the hole Fermi surface (up to 35 T for  $x = 2.5\%$  and 5%, up to 45 T for  $x = 7.5\%$ ); the oscillations from the hole orbits are likely suppressed due to the disorder scattering introduced with Cd impurities. This smearing may be stronger for hole than for electron orbits as a consequence of their larger effective masses<sup>39,40</sup>. The electron Fermi surface in  $\text{CeCo}(\text{In}_{1-x}\text{Cd}_x)_5$  also shrinks ( $F_3$  de-

creases with  $x$ ), and we can safely interpret this as the effect of hole doping in analogy with  $\text{LaCo}(\text{In}_{1-x}\text{Cd}_x)_5$ . Note that the reduction of the volume of the electron FS sheet corresponding to the decrease of  $F_3$  is very modest and accounts for only  $\sim 1/30$  of the hole introduced by Cd (see Appendix). Therefore it is likely that the added hole is mainly distributed over the parts of the Fermi surface which we do not observe in  $\text{CeCo}(\text{In}_{1-x}\text{Cd}_x)_5$ . Since the effective masses<sup>39</sup> and the hybridization gap<sup>47</sup> are known to be anisotropic, we cannot exclude that the chemical shift due to Cd leads to a more dramatic volume change on the hole sheet of the FS, and that this change creates nesting conditions. Note that the suppression of the  $F_4$  and  $F_5$  electron orbits with Cd in both the Ce and La compounds may indicate a more cylindrical (less corrugated along the  $c$ -axis) electron sheet. Perhaps such small changes in corrugation also lead to improved nesting along the  $c$ -axis. Since the wave vector remains commensurate in the plane  $(1/2, 1/2)$ , and it is only the  $c$ -axis component that becomes commensurate in Cd doped  $\text{CeCoIn}_5$ , as compared to pure  $\text{CeRhIn}_5$ <sup>43</sup>, small changes in the Fermi surface may indeed cause this lock onto commensurability.

## V. THE EFFECTIVE MASS AND THE MEAN FREE PATH

Figure 7 shows the dHvA amplitudes as a function of temperature for the  $F_3$  and  $F_4$  orbits in  $\text{CeCo}(\text{In}_{1-x}\text{Cd}_x)_5$ . As the temperature is increased, the Landau levels are broadened, and the dHvA oscillations suppressed. This suppression is well described by the Lifshitz-Kosevich (LK) formula<sup>33</sup>:

$$A(T, H) = A_0 \frac{X_T}{\sinh(X_T)},$$

with  $X_T = \frac{\alpha m^* T}{m_e H}$ , where  $A$  is the dHvA amplitude,  $A_0$  the  $T = 0$  amplitude,  $m^*$  the effective mass,  $m_e$  the bare electron mass, and  $\alpha = \frac{\pi^2 k_B}{\mu_B} = 14.69$  T/K. The fit to the LK expression (see solid lines in figure 7) allows the determination of the effective cyclotron mass  $m^*$  for each orbit. The values obtained for  $m^*$  are  $6.8 \pm 0.2$ ,  $5.9 \pm 0.4$ , and  $7.7 \pm 0.4$  (in units of the bare electron mass  $m_0$ ) for the  $F_3$  branch in the  $x = 2.5\%$ ,  $5\%$  and  $7.5\%$  samples, and  $m^* = 12.3 \pm 0.2$  for the  $F_4$  branch in the  $x = 2.5\%$  sample, as listed in Fig. 7 and table I. These are close to, but smaller than, the values of  $8.4 m_0$  and  $18 m_0$  previously determined for  $F_3$  and  $F_4$  from dHvA measurements along the same orientation ( $H \parallel [001]$ ) in pure  $\text{CeCoIn}_5$ <sup>39</sup>. The cyclotron effective masses in  $\text{LaCo}(\text{In}_{1-x}\text{Cd}_x)_5$  have not been investigated in this study and are assumed to be comparable to the values found in pure  $\text{LaCoIn}_5$ <sup>41</sup>.



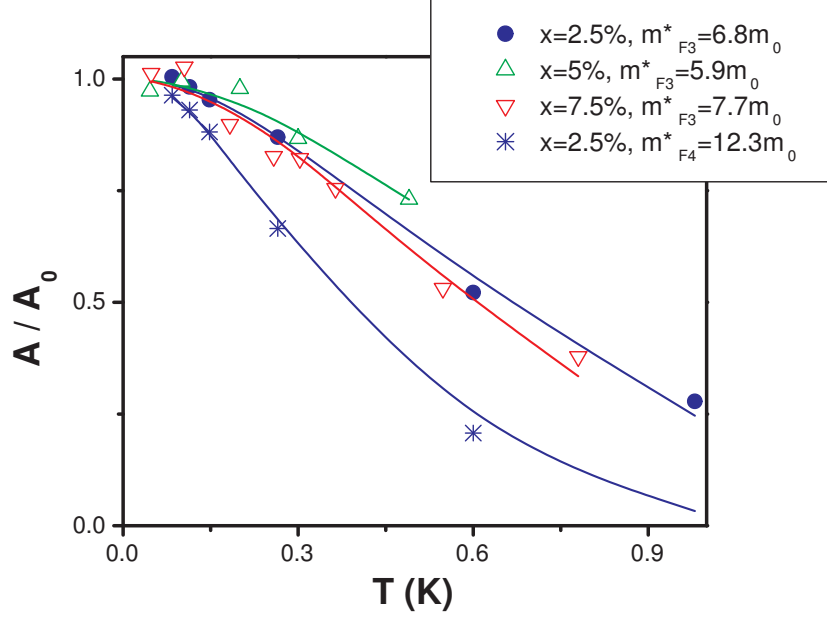


FIG. 7: (Color online) Normalized dHvA amplitude vs Temperature in  $\text{CeCo}(\text{In}_{1-x}\text{Cd}_x)_5$ . The amplitudes shown correspond to the dHvA branches  $F_3$  ( $\bullet$ ) and  $F_4$  ( $*$ ) for  $x = 2.5\%$ ,  $F_3$  ( $\triangle$ ) for  $x = 5\%$ , and  $F_3$  ( $\nabla$ ) for  $x = 7.5\%$ . Solid lines are fits of the Lifshitz-Kosevich formula to the data (see text).

The most striking result of this analysis is the absence of mass enhancement at the critical concentration  $x_c = 7.5\%$ , at odds with the presence of an AFM quantum critical point in the phase diagram. Given the contrasting effect of pressure and Cd doping in this system, and given that pressure is known to suppress  $m^*$  in pure  $\text{CeCoIn}_5$ <sup>48</sup>, one would naively expect Cd to enhance  $m^*$ . Similar to our results, no mass enhancement is observed via dHvA measurements in Rh doped  $\text{CeCoIn}_5$ <sup>46</sup>, in which no change in the Fermi surface is observed at the onset of AFM order. The absence of mass enhancement with Cd doping may be simply due to the high magnetic fields used for detecting dHvA oscillations and known to be detrimental to  $m^*$ . We also cannot exclude a mass enhancement for fields applied in-plane, nor for the hole sheets of the Fermi surface, as we have only been able to determine  $m^*$  for  $H \parallel [001]$  on the lightest part of the Fermi surface, namely the largest electron sheet. The lack of mass enhancement near the QCP is similar to the case of Cr where the QCP is not accompanied by a large carrier mass enhancement. This has been shown to be due to the small phase space occupied by the exchange enhanced magnetic fluctuations<sup>49</sup>.

In contrast, dHvA measurements on  $\text{CeRhIn}_5$  under pressure reveal a drastic change to

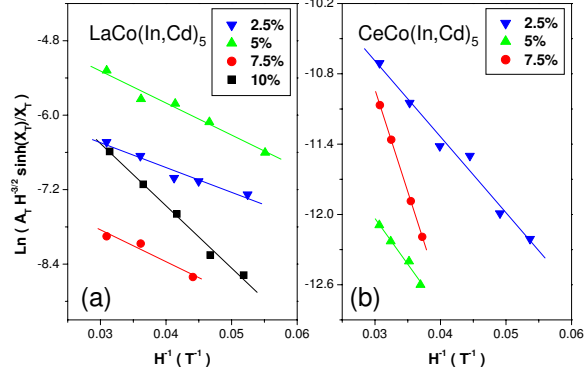


FIG. 8: (Color online) Dingle Plot. Reduced amplitude (see text) vs inverse magnetic field in (a)  $\text{LaCo}(\text{In}_{1-x}\text{Cd}_x)_5$  and (b)  $\text{CeCo}(\text{In}_{1-x}\text{Cd}_x)_5$  for indicated nominal Cd concentration. Solid lines are linear fits that determine the Dingle temperature,  $T_D$ .

the Fermi surface, with diverging effective masses, at the pressure required to suppress the antiferromagnetic state<sup>50</sup>. In light of these results, the absence of mass enhancement in  $\text{CeCo}(\text{In}_{1-x}\text{Cd}_x)_5$  at  $x_c = 7.5\%$  may be related to the absence of significant changes to the light mass Fermi surface sheets and indicate the possibility of strong fluctuation scattering only on specific sections of the Fermi surface. These are known as hot spots and we may not be observing these specific FS regions in our investigation. Such hot spots, where the cyclotron effective mass diverges, have been previously reported in cubic  $\text{CeIn}_3$ <sup>51</sup>. The large ordered moment in  $\text{CeCo}(\text{In}_{1-x}\text{Cd}_x)_5$  of  $\sim 0.7\mu_B$  per Ce<sup>28</sup> for  $x > x_c$  suggests that the purported SDW transition opens a gap over a large fraction of the FS and, further, that the precursor fluctuations in the paramagnetic state may make it difficult to observe the parts of the FS involved even at high field. This may explain the absence of dHvA oscillations for much of the FS (both hole and electron FS) for  $x > 2.5\%$  as large fractions of the FS may be involved in the nesting associated with the SDW-like state. Recently, hot spots at particular regions of the hole FS of  $\text{Ce}(\text{Rh},\text{Co})\text{In}_5$  have been suggested to explain the commensurate,  $Q = (1/2, 1/2, 1/2)$ , AFM order that has been observed between Rh concentrations of 25 and 60%(Ref. 52).

Landau levels are also broadened by impurity scattering of the quasiparticles. In the Lifshitz-Kosevich theory, the associated amplitude reduction factor is the so-called Dingle factor,  $\exp(-\frac{2\pi^2 k_B T_D}{\beta H})$ , where  $k_B$  is the Boltzmann factor, and  $\beta = g \mu_B \frac{m_0}{m^*}$  with  $g$  the Landé factor. The Dingle temperature,  $T_D$ , is defined as  $T_D = \frac{\hbar}{2\pi k_B \tau}$  with  $\tau^{-1}$  the impurity

TABLE I: Effective mass ( $m^*$ ), Dingle temperature ( $T_D$ ), mean free path ( $\ell$ ) and residual resistivity ratio (RRR) in  $\text{LaCo}(\text{In}_{1-x}\text{Cd}_x)_5$  and  $\text{CeCo}(\text{In}_{1-x}\text{Cd}_x)_5$ .

	$x(\%)$	$m^*(m_0)$	$T_D(\text{K})$	$\ell$ (nm)	RRR
$\text{LaCo}(\text{In}_{1-x}\text{Cd}_x)_5$	2.5		2.71	186	58
	5		3.50	143	36
	7.5		3.48	144	26
	10		6.81	73	16
$\text{CeCo}(\text{In}_{1-x}\text{Cd}_x)_5$	2.5	6.8	0.64	119	
	5	5.9	0.89	98	
	7.5	7.7	1.53	43	

scattering rate<sup>33</sup>. Experimentally,  $T_D$  is determined from the slope of the reduced amplitude,  $\ln(\frac{A_T}{H^{3/2}} \frac{\sinh(X_T)}{X_T})$ , vs inverse magnetic field,  $H^{-1}$ , where  $A_T$  is the dHvA amplitude measured at the lowest temperature (0.1 K for  $\text{CeCo}(\text{In}_{1-x}\text{Cd}_x)_5$  and 0.3 K for  $\text{LaCo}(\text{In}_{1-x}\text{Cd}_x)_5$ ). The Dingle plots in both systems are shown in Fig. 8. This allows an estimation of the mean free path defined as  $\ell = v_F \tau$ , where  $v_F$  is the Fermi velocity, given by  $v_F = \frac{\hbar k_F}{m^*}$  with  $k_F$  related to the dHvA frequency  $F$  through the Onsager relation:  $2eF = \hbar k_F^2$  ( $e$  being the electronic charge). We have used the frequencies of  $F_3$  shown in Fig. 6 to determine  $k_F$  and the mean free path  $\ell$  for this orbit for  $H \parallel [001]$  in both  $\text{LaCo}(\text{In}_{1-x}\text{Cd}_x)_5$  and  $\text{CeCo}(\text{In}_{1-x}\text{Cd}_x)_5$ . The results of  $T_D$  and  $\ell$  are summarized in table I together with  $m^*$ . The values obtained by us are consistent with the previously reported<sup>41</sup>  $\ell \simeq 200$  nm and 70 nm in  $\text{LaCoIn}_5$  and  $\text{CeCoIn}_5$  respectively. We found that in both compounds there is a systematic suppression of the mean free path due to disorder scattering introduced by the Cd substitution. A similar suppression is observed in the residual resistivity ratios (RRR) with increasing Cd concentrations for  $\text{LaCo}(\text{In}_{1-x}\text{Cd}_x)_5$  (see table I), with the RRR defined as the ratio of the zero field resistivity at 300 and 3 K (not shown). The RRR values in  $\text{CeCo}(\text{In}_{1-x}\text{Cd}_x)_5$  do not directly reflect the degree of disorder in the material due to the presence of the coherence peak and therefore they have been omitted in table I.

## VI. DISCUSSION AND CONCLUSIONS

The most obvious effects of Cd substitution into  $\text{CeCoIn}_5$  and  $\text{LaCoIn}_5$  that our data reveal are the systematic lattice contraction, as we established with X-ray diffraction, and the chemical potential shift due to the hole doping as apparent from the analysis of our dHvA data in  $\text{LaCo}(\text{In},\text{Cd})_5$ . We demonstrated that for  $\text{LaCo}(\text{In},\text{Cd})_5$  the dHvA frequencies associated with the main electron Fermi surface sheet decrease, while those of the hole sheet increase in a manner consistent with hole doping with Cd substitution. In addition, we demonstrated that a dHvA frequency associated with the electron sheet of Cd doped  $\text{CeCoIn}_5$ , which is the only piece of the Fermi surface resolved in our dHvA data, decreases at a rate similar to the La analog, again consistent with that expected for a small density of doped holes. The corresponding change in the electron FS volume only accounts for 1/30 of the doped hole/Cd, suggesting that the added holes are mainly distributed over the remaining pieces of the Fermi surface, which we do not observe. Overall, the Fermi surface of  $\text{CeCo}(\text{In}_{1-x}\text{Cd}_x)_5$  remains closely related that of pure  $\text{CeCoIn}_5$ , with only modest changes in the dHvA frequencies and cyclotron masses, despite the dramatic evolution of the zero field ground state from superconducting to superconducting+antiferromagnetic. The similarity of the changes that occur with doping in the La and Ce compounds allows us to rule out any substantial  $f$ -electron localization and, thus, to rule out mechanisms for the antiferromagnetic state that rely on local moment formation. It follows that the commensurate AFM order in  $\text{CeCo}(\text{In}_{1-x}\text{Cd}_x)_5$  is likely due to an itinerant, SDW-type, mechanism which relies on FS nesting. The most famous example of SDW ordering that is commensurate with the underlying lattice is the elemental antiferromagnet Cr which, although incommensurate when pure, evolves to a commensurate state with small Mn doping<sup>29</sup>.

Our dHvA data are also similar to that of Rh doped  $\text{CeCoIn}_5$ <sup>46</sup> where the FS is seen to undergo small changes so that a large Fermi surface is observed in both Cd and Rh doped  $\text{CeCoIn}_5$ . Thus, for both Cd and Rh substitution into  $\text{CeCoIn}_5$  commensurate AFM order coexisting with superconductivity is observed along with a Fermi surface that appears to contain a substantial contribution from the Ce  $4f$ -electrons. The main difference in these two substitution series is that Cd substitution suppresses superconductivity<sup>25</sup> for concentrations beyond 15%, while superconductivity remains apparent up to 60% Rh substitution<sup>31</sup>. The stronger suppression of superconductivity with Cd may be the consequence of in-plane

impurity scattering.

However, there are several aspects of Cd doped  $\text{CeCoIn}_5$  that remain poorly understood. It is well known that pressure applied to  $\text{CeCo}(\text{In}_{1-x}\text{Cd}_x)_5$  causes a return to paramagnetism and an increase of the superconducting critical temperature so that pressure appears to reverse the most obvious consequences of Cd doping<sup>25</sup>. If the main effect of Cd doping into  $\text{CeCoIn}_5$  is a shift of the chemical potential caused by the addition of holes as our data suggest, then it is difficult to account for the reversible tuning of the AFM order with pressure. For any reasonable value for the compressibility of Cd doped  $\text{CeCoIn}_5$  the carrier density change with experimentally accessible pressures would be very small. Thus, it is unlikely that pressure simply reverses the changes that occur with Cd doping. This suggests that there are subtle changes that occur to  $\text{CeCoIn}_5$  with doping or pressure that are more likely associated with the Kondo effect and the formation of the heavy fermion metallic state. A second, perhaps related important open question, and perhaps a clue to the origin of the AFM order, is why the magnetic structure is commensurate, with the same wavevector,  $Q = (1/2, 1/2, 1/2)$ , as the neutron scattering resonance observed in superconducting, nominally pure,  $\text{CeCoIn}_5$ <sup>20</sup>. In addition, the lack of more direct evidence for SDW formation leaves open the possibility that the magnetic state in  $\text{CeCo}(\text{In}_{1-x}\text{Cd}_x)_5$  has a character intermediate between local moment or highly itinerant so that a simple description is difficult.

It appears from our data, as well as from the NMR results<sup>27</sup>, that Cd doping of  $\text{CeCoIn}_5$  into an AFM phase does not conform to the Doniach model<sup>2</sup> where the Kondo and RKKY coupling compete at a quantum critical point. Instead our data suggest that a more itinerant antiferromagnetism develops out of a Fermi surface which contains the hybridized Ce  $4f$ -electrons. The role of Cd for inducing this AFM order in  $\text{CeCoIn}_5$  remains elusive and the resolution of this mystery is likely to broaden our approach to quantum criticality beyond the Doniach phase diagram.

### Acknowledgments

We are thankful to E.C. Palm for his technical assistance with the use of dilution refrigerator. A portion of this work was performed at the National High Magnetic Field Laboratory, which is supported by NSF Cooperative Agreement No. DMR-0654118, by the

State of Florida, and by the DOE. L.B. is supported by DOE-BES. R.G.G. was supported directly by NSF. C.C. acknowledges ICAM fellowship. Z.F. acknowledges support through NSF Grant No. NSF-DMR-0503361. J. F. D. acknowledges support through NSF Grant No. NSF-DMR-084376. D.P.Y. acknowledges support through NSF Grant No. NSF-DMR-0449022. J.Y.C. acknowledges support through NSF Grant No. NSF-DMR-0756281. I. V. was supported in part by DOE Grant. No. DE-FG02-08ER46492.

## Appendix

We present below an estimation of the volume change of the electron Fermi surface in  $\text{CeCo}(\text{In}_{1-x}\text{Cd}_x)_5$  due to Cd within cylindrical Fermi surface approximation. We use the Onsager relation:

$$F = \frac{\hbar c}{e} A = \frac{1}{\pi} \Phi_0 A, \quad (\text{A.1})$$

where  $\Phi_0 = hc/2e = 2 \cdot 10^{-11} \text{T} \cdot \text{cm}^2$  is the flux quantum. The shift in the frequency of the  $F_3$  (electron) orbit,  $\delta F$ , translates into the change in the area of the extremal orbit, and allows for a rough estimate of the change in the volume of the Fermi surface via:

$$\delta V = \frac{2\pi}{l_c} \delta A = \frac{2\pi^2 \delta F}{l_c \Phi_0}. \quad (\text{A.2})$$

where  $l_c$  is the lattice constant along [001]. The number of states in this volume is (with a factor of 2 for spin degeneracy):

$$\delta n = \frac{2\delta V}{(2\pi)^3} = \frac{1}{2\pi} \frac{\delta F}{l_c \Phi_0}. \quad (\text{A.3})$$

Using experimental values of  $\delta f \approx 2.5 \cdot 10^2 \text{T}$  per 10% nominal Cd, and  $l_c = 7.6 \text{\AA}$ , we get  $\delta n \approx 2.6 \times 10^{19} \text{cm}^{-3}$ . The next step is to determine what fraction of 1 hole per Cd this change in density corresponds to. With a unit cell volume  $v_u \approx 161 \text{\AA}^3 = 1.6 \times 10^{-22} \text{cm}^3$  and given that each unit cell has  $5x$  holes, the density of added holes is:  $\frac{5x}{v_u} \approx 3.1x \times 10^{22} \text{cm}^{-3}$ . For nominal  $x = 0.1$  we expect the actual Cd concentration to be  $x \sim 0.03$ , so we should have  $\delta n \approx 9 \times 10^{20} \text{cm}^{-3}$ . In other words, the change in the electron Fermi surface volume

(estimated from the change in the  $F_3$  frequency) due to Cd only accounts for  $\sim 3\%$  of the additional hole, assuming that each Cd introduces one hole.

- 
- \* Present address: Department of Physics, George Washington University, Washington DC 20052
- † Present address: Department de Physique, Universite de Montreal, Montreal H3C 3J7 Canada
- ‡ Intel Corp.
- <sup>1</sup> P. Coleman, C. Pépin, Q. Si, and R. Ramazashvili, *Journal of Physics: Condensed Matter* **13**, R723 (2001).
- <sup>2</sup> S. Doniach, *Physica* **91B**, 231 (1977).
- <sup>3</sup> N. D. Mathur, F. M. Grosche, S. R. Julian, I. R. Walker, D. M. Freye, R. K. W. Haselwimmer, and G. G. Lonzarich, *Nature* **394**, 39 (1998).
- <sup>4</sup> P. Monthoux, D. Pines, and G. G. Lonzarich, *Nature* **450**, 1177 (2007).
- <sup>5</sup> J. Tallon, T. Benseman, G. Williams, and J. Loram, *Physica C: Superconductivity* **415**, 9 (2004).
- <sup>6</sup> F. Steglich, J. Aarts, C. D. Bredl, W. Lieke, D. Meschede, W. Franz, and H. Schäfer, *Phys. Rev. Lett.* **43**, 1892 (1979).
- <sup>7</sup> H. R. Ott, H. Rudigier, Z. Fisk, and J. L. Smith, *Phys. Rev. Lett.* **50**, 1595 (1983).
- <sup>8</sup> C. Petrovic, P. G. Pagliuso, M. F. Hundley, R. Movshovich, J. L. Sarrao, J. D. Thompson, Z. Fisk, and p Monthoux, *J. Phys. : Condens. Matter* **13**, L337 (2001).
- <sup>9</sup> K. Kuga, Y. Karaki, Y. Matsumoto, Y. Machida, and S. Nakatsuji, *Phys. Rev. Lett.* **101**, 137004 (2008).
- <sup>10</sup> Y. Ihara, H. Takeya, K. Ishida, C. Michioka, K. Yoshimura, K. Takada, T. Sasaki, H. Sakurai, and E. Takayama-Muromachi, *Journal of Physics and Chemistry of Solids* **68**, 2119 (2007).
- <sup>11</sup> J. Dai, Q. Si, J.-X. Zhu, and E. Abrahams, *Proceedings of the National Academy of Science* **106**, 4118 (2009).
- <sup>12</sup> Y. Maeno, H. Hashimoto, K. Yoshida, S. Nishizaki, T. Fujita, J. Bednorzt, and F. Lichtenberg, *Nature* **372**, 532 (1994).
- <sup>13</sup> C. Pfleiderer, *Rev. Mod. Phys.* **81**, 1551 (2009).
- <sup>14</sup> T. Shibauchi, L. Krusin-Elbaum, M. Hasegawa, Y. Kasahara, R. Okazaki, and Y. Matsuda, *Proceedings of the National Academy of Science* **105**, 7120 (2008).

- <sup>15</sup> S. Nakatsuji, D. Pines, and Z. Fisk, *Phys. Rev. Lett.* **92**, 016401 (2004).
- <sup>16</sup> J. Paglione, T. A. Sayles, P.-C. Ho, J. R. Jeffries, and M. B. Maple, *Nat. Phys.* **3**, 706 (2007).
- <sup>17</sup> A. Bianchi, R. Movshovich, I. Vekhter, P. G. Pagliuso, and J. L. Sarrao, *Phys. Rev. Lett.* **91**, 257001 (2003).
- <sup>18</sup> J. Paglione, M. A. Tanatar, D. G. Hawthorn, E. Boaknin, R. W. Hill, F. Ronning, M. Sutherland, L. Taillefer, C. Petrovic, and P. C. Canfield, *Phys. Rev. Lett.* **91**, 246405 (2003).
- <sup>19</sup> S. Singh, C. Capan, M. Nicklas, M. Rams, A. Gladun, H. Lee, J. F. DiTusa, Z. Fisk, F. Steglich, and S. Wirth, *Phys. Rev. Lett.* **98**, 057001 (2007).
- <sup>20</sup> C. Stock, C. Broholm, J. Hudis, H. J. Kang, and C. Petrovic, *Phys. Rev. Lett.* **100**, 087001 (2008).
- <sup>21</sup> B.-L. Young, R. R. Urbano, N. J. Curro, J. D. Thompson, J. L. Sarrao, A. B. Vorontsov, and M. J. Graf, *Phys. Rev. Lett.* **98**, 036402 (2007).
- <sup>22</sup> M. Kenzelmann, T. Strassle, C. Niedermayer, M. Sigrist, B. Padmanabhan, M. Zolliker, A. D. Bianchi, R. Movshovich, E. D. Bauer, J. L. Sarrao, et al., *Science* **321**, 1652 (2008).
- <sup>23</sup> J. Spehling, R. H. Heffner, J. E. Sonier, N. Curro, C. H. Wang, B. Hitti, G. Morris, E. D. Bauer, J. L. Sarrao, F. J. Litterst, et al., *Phys. Rev. Lett.* **103**, 237003 (2009).
- <sup>24</sup> E. D. Bauer, C. Capan, F. Ronning, R. Movshovich, J. D. Thompson, and J. L. Sarrao, *Phys. Rev. Lett.* **94**, 047001 (2005).
- <sup>25</sup> L. D. Pham, T. Park, S. Maquilon, J. D. Thompson, and Z. Fisk, *Phys. Rev. Lett.* **97**, 056404 (2006).
- <sup>26</sup> C. Adriano, C. Giles, E. M. Bittar, L. N. Coelho, F. de Bergevin, C. Mazzoli, P. L., W. Ratcliff, R. Bindel, J. W. Lynn, et al., *arXiv.org:0912.4467* (2009).
- <sup>27</sup> R. R. Urbano, B.-L. Young, N. J. Curro, J. D. Thompson, L. D. Pham, and Z. Fisk, *Phys. Rev. Lett.* **99**, 146402 (2007).
- <sup>28</sup> M. Nicklas, O. Stockert, T. Park, K. Habicht, K. Kiefer, L. D. Pham, J. D. Thompson, Z. Fisk, and F. Steglich, *Phys. Rev. B* **76**, 052401 (2007).
- <sup>29</sup> E. E. Fawcett, H. L. Alberts, V. Y. Galkin, D. R. Noakes, and J. V. Yakhmi, *Rev. Mod. Phys.* **66**, 25 (1994).
- <sup>30</sup> A. V. Chubukov and L. P. Gor'kov, *Phys. Rev. Lett.* **101**, 147004 (2008).
- <sup>31</sup> V. S. Zapf, E. J. Freeman, E. D. Bauer, J. Petricka, C. Sirvent, N. A. Frederick, R. P. Dickey, and M. B. Maple, *Phys. Rev. B* **65**, 014506 (2001).



- <sup>32</sup> Y. Tokiwa, R. Movshovich, F. Ronning, E. D. Bauer, P. Papin, A. D. Bianchi, J. F. Rauscher, S. M. Kauzlarich, and Z. Fisk, *Phys. Rev. Lett.* **101**, 037001 (2008).
- <sup>33</sup> D. Shoenberg, *Magnetic Oscillations in Metals*, Cambridge University Press (1984).
- <sup>34</sup> C. H. Booth, E. D. Bauer, A. D. Bianchi, F. Ronning, J. D. Thompson, J. L. Sarrao, J. Y. Cho, J. Y. Chan, C. Capan, and Z. Fisk, *Phys. Rev. B* **79**, 144519 (2009).
- <sup>35</sup> E. D. Bauer, F. Ronning, C. Capan, M. J. Graf, D. Vandervelde, H. Q. Yuan, M. B. Salamon, D. J. Mixson, N. O. Moreno, S. R. Brown, et al., *Phys. Rev. B* **73**, 245109 (2006).
- <sup>36</sup> J. R. Jeffries, N. A. Frederick, E. D. Bauer, H. Kimura, V. S. Zapf, K.-D. Hof, T. A. Sayles, and M. B. Maple, *Phys. Rev. B* **72**, 024551 (2005).
- <sup>37</sup> M. Nicklas, R. Borth, E. Lengyel, P. G. Pagliuso, J. L. Sarrao, V. A. Sidorov, G. Sparn, F. Steglich, and J. D. Thompson, *Journal of Physics: Condensed Matter* **13**, L905 (2001).
- <sup>38</sup> C. Capan, D. Hurt, G. Seyfarth, B. Prevost, S. Roorda, A. D. Bianchi, S. Nakatsuji, and Z. Fisk, arXiv:0912.0046 (2009).
- <sup>39</sup> R. Settai, H. Shishido, S. Ikeda, Y. Murakawa, M. Nakashima, D. Aoki, Y. Haga, H. Harima, and Y. Onuki, *J. Phys.: Condens. Matter* **13**, L627 (2001).
- <sup>40</sup> D. Hall, E. C. Palm, T. P. Murphy, S. W. Tozer, Z. Fisk, U. Alver, R. G. Goodrich, J. L. Sarrao, P. G. Pagliuso, and T. Ebihara, *Phys. Rev. B* **64**, 212508 (2001).
- <sup>41</sup> N. Harrison, U. Alver, R. G. Goodrich, I. Vekhter, J. L. Sarrao, P. G. Pagliuso, N. O. Moreno, L. Balicas, Z. Fisk, D. Hall, et al., *Phys. Rev. Lett.* **93**, 186405 (2004).
- <sup>42</sup> H. Shishido, R. Settai, D. Aoki, S. Ikeda, H. Nakawaki, N. Nakamura, T. Iizuka, Y. Inada, K. Sugiyama, T. Takeuchi, et al., *J. Phys. Soc. Jpn* **71**, 162 (2002).
- <sup>43</sup> W. Bao, P. G. Pagliuso, J. L. Sarrao, J. D. Thompson, Z. Fisk, J. W. Lynn, and R. W. Erwin, *Phys. Rev. B* **62**, R14621 (2000).
- <sup>44</sup> J. Jensen and M. A. R., Clarendon Press Oxford (1991).
- <sup>45</sup> D. Hall, L. Balicas, Z. Fisk, R. G. Goodrich, U. Alver, and J. L. Sarrao, *Phys. Rev. B* **79**, 033106 (2009).
- <sup>46</sup> S. K. Goh, J. Paglione, M. Sutherland, E. C. T. O'Farrell, C. Bergemann, T. A. Sayles, and M. B. Maple, *Phys. Rev. Lett.* **101**, 056402 (2008).
- <sup>47</sup> K. S. Burch, S. V. Dordevic, F. P. Mena, A. B. Kuzmenko, D. van der Marel, J. L. Sarrao, J. R. Jeffries, E. D. Bauer, M. B. Maple, and D. N. Basov, *Phys. Rev. B* **75**, 054523 (2007).
- <sup>48</sup> H. Shishido, R. Settai, S. Hashimoto, Y. Inada, and Y. Onuki, *J. Magn. Magn. Materials*

**272-276**, 225 (2004).

<sup>49</sup> S. M. Hayden, R. Doubble, G. Aeppli, T. G. Perring, and E. Fawcett, Phys. Rev. Lett. **84**, 999 (2000).

<sup>50</sup> H. Shishido, R. Settai, H. Harima, and Y. Onuki, J. Phys. Soc. Jpn **74**, 1103 (2005).

<sup>51</sup> T. Ebihara, N. Harrison, M. Jaime, S. Uji, and J. C. Lashley, Phys. Rev. Lett. **93**, 246401 (2004).

<sup>52</sup> S. Ohira-Kawamura, H. Shishido, A. Yoshida, R. Okazaki, H. Kawano-Furukawa, T. Shibauchi, H. Harima, and Y. Matsuda, Phys. Rev. B **76**, 132507 (2007).